Confirming TESS exoplanet candidates and searching for multi-planetary systems using transit photometry and timing variations

Allison Valji

Abstract

Determining the habitability of exoplanets, which are planets outside the Solar System, and studying multi-planetary star systems have long been the goals of many astronomers, but first exoplanets must be discovered. The Transiting Exoplanet Survey Satellite (TESS) is a space telescope that searches for exoplanets using the transit method, or the indirect observation of exoplanets via the change in brightness of the star when the planet passes in front. Transit observations can be displayed graphically on a light curve, or brightness over time graph. Once a transit is detected by TESS, the planet is considered to be an exoplanet candidate, but some candidates can turn out to be false positives rather than planets. This study used the Phillips 24" Telescope at the Mt. Lemmon SkyCenter Observatory to perform follow-up transit observations, and then used the open source software AstroImageJ to create light curves. The existence of exoplanets in the TOI-1858, TOI-1832, and TOI-3856 systems was confirmed. Possible transit timing variations were found in the TOI-1832 system, and a larger unknown object was found in the TOI-3856 system, indicating the potential existence of two multi-planetary systems. Also, the planetary radii of the targets and the criteria for a good comparison star were determined. Calculations for planet radii can be combined with future values for planet mass to determine the density of the newly confirmed planets, and the criteria for ideal comparison stars can be applied to future transit observations of these targets and others.

Keywords: exoplanets – transit method – TESS

1 Introduction

Over the past few decades research on exoplanets, or planets orbiting stars outside the Solar System, has drastically increased as researchers seek to understand these planets and search for potentially habitable ones. Much of this research has become possible due to telescopes like the Transiting Exoplanet Survey Satellite[1] (TESS) which is specifically designed for detecting exoplanets. TESS uses the transit method, which is an indirect way of observing exoplanets by measuring the brightness of the star (Fig. 1). As an exoplanet orbits a star, it passes between the star and the observer, and a portion of the star's light is temporarily blocked in what is called a transit. When a planet transits, the overall brightness of the star decreases which enables researchers to detect the presence of exoplanets by measuring decreases in stellar brightness. Graphically, a transit can be displayed using a light curve or a graph that shows brightness over time. If an exoplanet is transiting, the light curve should show one singular dip in brightness.

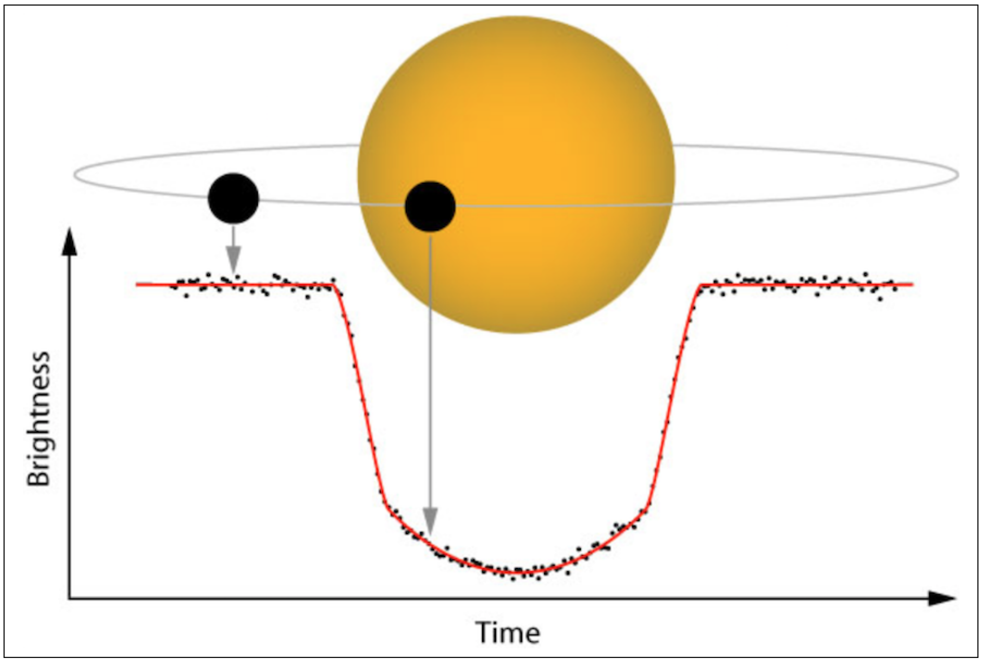

Figure 1. Diagram[2] showing an exoplanet transit. When the planet orbits the star it temporarily passes between the star and the observer blocking a portion of the star's light. This blocking of light, or transit, causes a singular small percentage decrease in brightness of the star which allows exoplanets to be indirectly detected. A transit can be graphically displayed as a light curve or brightness over time graph.

When TESS detects a star with a dip in brightness that star is considered to contain an exoplanet candidate, but is not completely confirmed to exist because the star could be a false positive. A false positive is a candidate whose star does contain fluctuations in brightness, but that change is not the result of a planet transiting. There have been many TESS exoplanet candidates in the past that have turned out to be false positives[3], such as eclipsing binary stars. Therefore, exoplanet candidates must be confirmed with follow-up ground-based transit observations.

Additionally, transit observations can be used to look for transit timing variations. Transit timing variations occur when there are differences between the expected time of transit and actual time of transit. So the predicted time of ingress (inital dip in brightness) and egress (final return to normal brightness) are different from the observed times. The actual time of transit is known based on initial TESS observations[4] and the calculated ephemeris. An ephemeris is the calculated position at given times based on known elements of the planet's orbit. So if transit timing variations are found, then there must be some other object–

potentially an additional planet in the system–that is gravitationally pulling on the first planet causing its orbit to speed up or slow down due to consequential changes in orbital shape. As a result, the time of transit happens earlier, or later, than expected.

The search for exoplanets, through both candidate confirmation with follow-up observations and transit timing variations, is important because it is the first step in future exoplanet research. If researchers want to search for habitable planets by looking at the atmospheres and compositions of exoplanets using telescopes like the James Webb Space Telescope[5] (JWST), or if they want to study the orbital architectures of multiplanetary systems, then this study must first be completed. Exoplanet research is so important because it helps researchers understand the origins of planetary formation and understand our Solar System especially when studying multi-planetary systems such as the ones found using transit timing variations. Devoting telescope time with an expensive resource like JWST, or studying a multi-planetary system, cannot be justified unless the exoplanet is first confirmed or the system is confirmed to have more than one planet with transit timing variations. It is risky to devote expensive resources to a planet that may not exist.

This paper will present transit observations of the following target stars containing exoplanet candidates: TOI-3856, TOI-1858, and TOI-1832. All targets were first observed in the TESS Prime Mission[6] but TOI-3856 was not determined to contain an exoplanet candidate until the Quick Look Pipeline Faint-star Search[7]. It will be determined if the TESS exoplanet candidates exist, and if there are transit timing variations present in the systems. Additionally, calculated planetary radii of the three exoplanet candidates and an analysis of the impact of the selection of comparison stars on light curves will be presented. Comparison stars are stars that are nearby the target star (e.g. Fig. 9) that are used as a reference to measure the target star's relative change in brightness. However, which stars are selected can change the light curve produced, so this study will analyze the impact of that choice.

2 Methods

2.1 Target Selection

To select the target stars in this study, a service that predicts when all known exoplanets and exoplanet candidates may be transiting, called Swarthmore Transit Finder[10], was used. Three target stars were chosen for meeting the following parameters:

1. Stars that contain TESS exoplanet candidates
2. Stars that have a bright enough magnitude for the telescope being used (< 13)
3. Stars that have a great enough transit depth, or change in brightness, to be detectable (> 7 ppt; parts per thousand)
4. Stars with a transit duration under 2.5 hours so the observation period is not too long

5. Stars with an orbital period close to a whole number so they transit at nighttime, on earth, frequently

6. Stars with transits visible in Tucson, Arizona from April to June 2024

Then, once the targets TOI-3856, TOI-1858, and TOI-1832 were selected, information from Swarthmore Transit Finder[10] was collected. First, the predicted times of transit were gathered in order to know what days and times the three candidates were predicted to transit. These times were calculated based on data from initial TESS observations[4]. Also, astronomical coordinates of each star in the form of right ascension and declination were collected in order to know where to point the telescope during the time of transit. Finally, stellar finder charts (Fig. 2) were downloaded so that the target stars could be identified in the field of stars seen in the images taken with the telescope and camera.

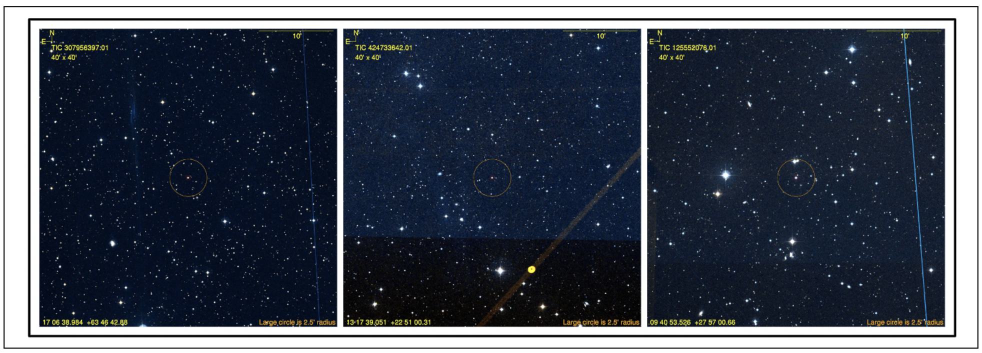

Figure 2. Finder Charts[10] for TOI-1858 (left), TOI-1832 (middle), and TOI-3856 (right) used to locate target stars in images taken by telescope. The charts are in a 40 arcsec-by-40 arcsec frame with orientation listed in the top left of each chart.

2.2 Observations and Data Collection

Observations took place at the Mt. Lemmon SkyCenter Observatory in Tucson, Arizona using the Phillips 24" Telescope and an attached QHY600 imaging camera with a red filter to reduce atmospheric noise and filter out moonlight. The telescope was controlled with a computer which was remotely logged into so the observations could be conducted without having to physically be at the observatory. Each target star was observed one to three times using the following procedure.

To begin, the Phillips 24" Telescope was pointed at the previously collected astronomical coordinates of the target star. Then, an initial image was taken to ensure the target star could be identified. The initial image was manually compared to the target star's finder charts in order to identify the target star in the initial images. At the same time, the initial image was uploaded to the website Astrometry.net[11] which determined the exact astronomical coordinates of the image, so that minor adjustments (approximately 10 arcsec at a time) could be made. If adjustments were necessary, then using Astrometry.net ensured the target star was in frame and easy to spot manually. Once the target star was found then an exposure time was set based on a "seeing profile" (e.g. Fig. 9), to maximize the amount of light read by the camera without saturation of pixels. Next, the camera was set to take images at the determined exposure time, and with a red filter, for the duration of the transit plus one hour before and after the predicted time of transit to account for timing variations, and to provide a pre- and post-transit brightness.

Finally, after these science images (normal non-calibration images) were taken, then three different types of calibration images–which are images that help reduce noise and eliminate systematic error in the data to increase precision of the light curve–were taken. Dark frames were taken with the shutter closed but with the same exposure time as the science images to account for thermal properties of the camera. Bias frames were taken with the shutter closed and the minimal possible exposure time to account for readout noise at the detector. Flat frames were taken with the camera pointed at an evenly illuminated surface with the telescope dome closed to account for differences in how each pixel responds to light due to imperfections in the light path.

TOI-3856 was observed on three different days: April 20, April 22, and April 24 of 2024. It was observed three times because of peculiarities found after initial data reduction of the data from April 20. On April 20, 267 images were taken of TOI-3856 with an exposure time of 40 seconds. On April 22, 316 images were taken of TOI-3856 with an exposure time of 40 seconds. On April 24, 373 images were taken of TOI-3856 with an exposure time of 40 seconds. On each night of observation 30 of each type of calibration frame were taken after observing. The reason there are a different number of images taken for each set of data, despite it being the same target star, is that the period of observation was sometimes a little more than one hour before and after transit, and because sometimes there was a programmed delay between images so there wouldn't be too much data. TOI-1858 and TOI-1832 were both observed once with 256 and 169 science images taken, respectively, and the same number of calibration images taken as with TOI-3856. TOI-1858 was observed on June 1, 2024 and TOI-1832 was observed on the same night as the first TOI-3856 observations, April 20, 2024. Images for both targets were taken with an exposure time of 60 seconds.

2.3 Data Reduction Using AstroImageJ

To turn the raw data into light curves the software AstroImageJ[8] was used. First, AstroImageJ was used to align the images of all five data sets to ensure that the target stars were in the same location in each image because telescope tracking is not perfect. Then, AstroImageJ was used to calibrate the data sets with dark, bias, and flat frames to reduce noise in the data. After completing these two steps, multi-aperture photometry was performed–which measures the relative flux in brightness or the brightness of the target star compared to the background brightness using nearby stars called comparison stars–for each set of data to plot each image on a light curve. Two comparison stars were chosen for TOI-1858 and TOI-1832, each, after a little experimentation with which stars provided the least noise in the light curve. This was determined by the light curve with the lowest Root Mean Square (RMS) value on the transit depth. After the multi-aperture photometry produced a light curve for each target (Fig. 3; Fig. 4), AstroImageJ features could be used to "smooth" the data using binning, or the averaging of data points together, and plot a line of best fit through the curve. Also, AstroImageJ could be used to plot the predicted time of ingress and egress (beginning and end of the dip in brightness) and to plot the comparison stars. This process was used again for the three TOI-3856 data sets to produce three light curves with the most noise-reducing set of comparison stars (Fig. 5; Fig. 6; Fig. 7). However, for TOI-3856, the choice of comparison stars seemed to greatly impact the resulting light curve so additional light curves were made (Fig. 9; Fig. 10; Fig. 11) with different sets of comparison stars in order to analyze the impact the selection of comparison stars has on the light curves.

2.4 Analyzing the Light Curves

In order to confirm the existence of these three exoplanet candidates, the shapes of the light curves were analyzed[12]. A transiting exoplanet has one singular dip in brightness while a false positive such as a variable star has periodic and oscillating fluctuations in brightness. Also, in order to search for timing variations, the predicted lines of ingress and egress plotted on the light curve were compared to the actual time of ingress and egress displayed in the light curve. Since these observations took place three years after the initial observations by TESS[6], the impact of any timing variations was large enough to be clearly visible in the light curves.

3 Results

3.1 Candidate Confirmation

The light curve of TOI-1858 (Fig. 3) showed one singular dip in brightness and no differences in timing from the lines of predicted ingress and egress. Therefore, it can be concluded that TOI-1858 is not a false positive and does indeed contain an exoplanet, but there are no transit timing variations over the course of the three years.

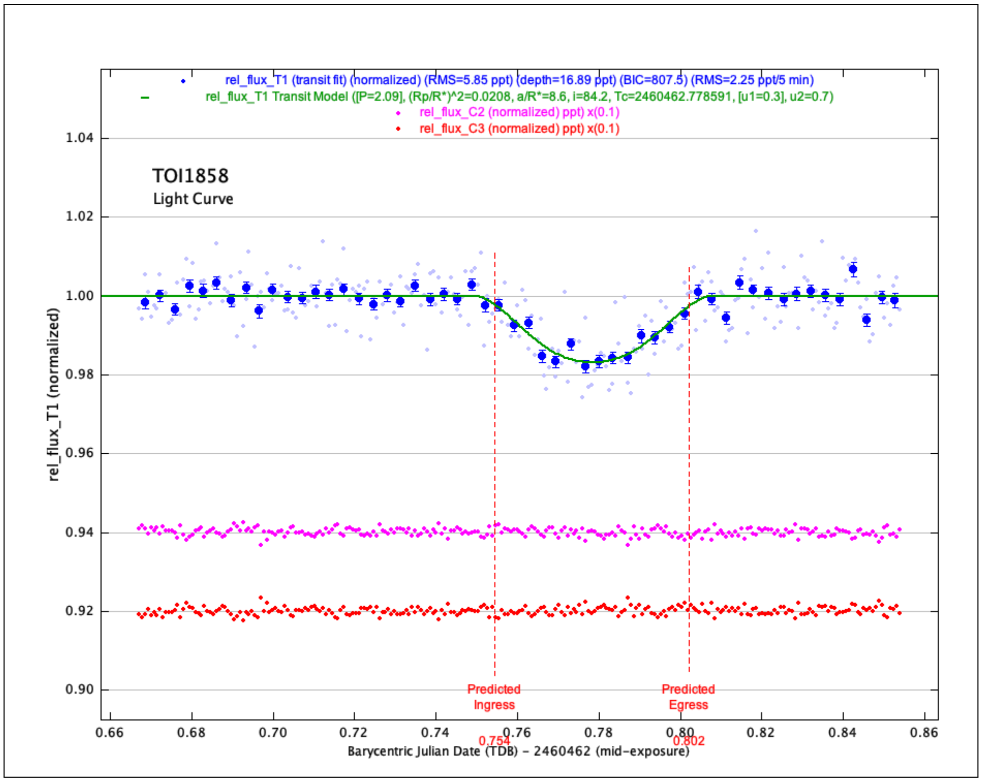

Figure 3. Light curve of TOI-1858 from observations on June 1, 2024. The curve shows brightness over time and is normalized to 1. Faint blue points represent each image, and the large blue points are binned with BinSize = 5 min and error bars. The curve is plotted with a line of best fit, predicted times of ingress and egress, and arbitrarily scaled/shifted plots of the comparison stars. The curve shows a singular dip in brightness and no transit timing variations.

The light curve of TOI-1832 (Fig. 4) also showed one singular dip in brightness, so TOI-1832 is also confirmed to contain an exoplanet and not a false positive. The possibility of transit timing variations can be seen in the light curve (Fig. 5), as the lines of ingress/egress begin and end earlier than expected, but there is some uncertainty in the data. Since the comparison stars' brightnesses are not flat, as one slopes up and the other slopes down, and there is some noise at the time of ingress/egress, the existence of timing variations cannot be determined for certain. Therefore, future observations are necessary to confirm the existence of timing variations. But if timing variations can be confirmed then that would indicate the existence of a multi-planetary system because there is an additional body gravitationally pulling on the first, causing the transit to occur earlier than predicted three years prior.

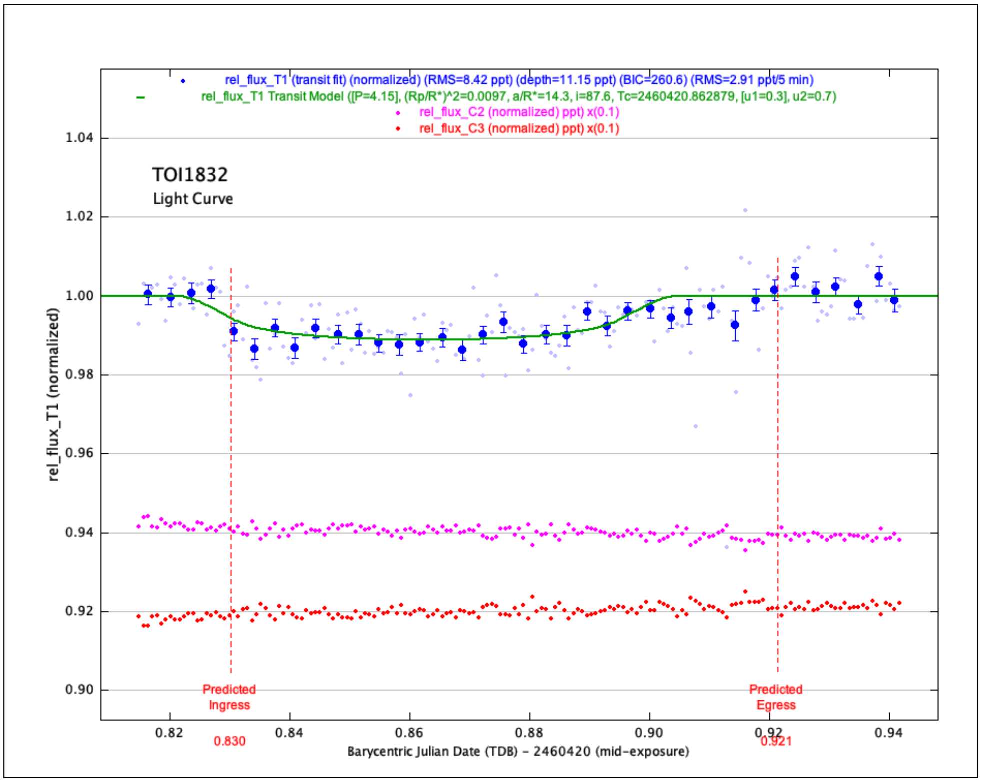

Figure 4. Light curve of TOI-1832 from observations on April 20, 2024. The curve shows brightness over time and is normalized to 1. Faint blue points represent each image, and the large blue points are binned points with BinSize = 5 min and error bars. The curve is plotted with a line of best fit, predicted times of ingress and egress, and arbitrarily scaled/shifted plots of the comparison stars. The curve shows a singular dip in brightness and variations between the predicted lines of ingress/egress and the actual times of ingress/egress. However, the variations in timing of ingress/egress occur at parts of the light curve where there is noise in the data. Also, one comparison star's (red) brightness slopes up and the other comparison star's (pink) brightness slopes down.

Finally, in the TOI-3856 light curves, each of the three curves shows a very different shape. The observations from April 20 (Fig. 5) display one large increase in brightness; the observations from April 22 (Fig. 6) display one singular dip in brightness as expected; and the observations from April 24 (Fig. 7) display one large decrease in brightness. Each light curve was created using the same comparison stars which provided the least amount of noise, or the lowest RMS value on transit depth.

Since the transit depth (change in brightness) from Fig. 5 and Fig. 7 is larger than the predicted transit depth and the depth in Fig. 6, it can be concluded that the depth in the April 20 and April 24 observations is the result of an additional larger body nearby passing in front of the target star, rather than transit timing variations. In both these cases, either the ingress or egress is missing, showing that this larger body does not transit at the same time/for the same duration as the first exoplanet, and therefore the object does not transit in the April 22 observations. However, because there is one singular dip in brightness close to the predicted transit depth of 1.3%[4] in Fig. 6, it can be confirmed that TOI-3856 contains an exoplanet candidate.

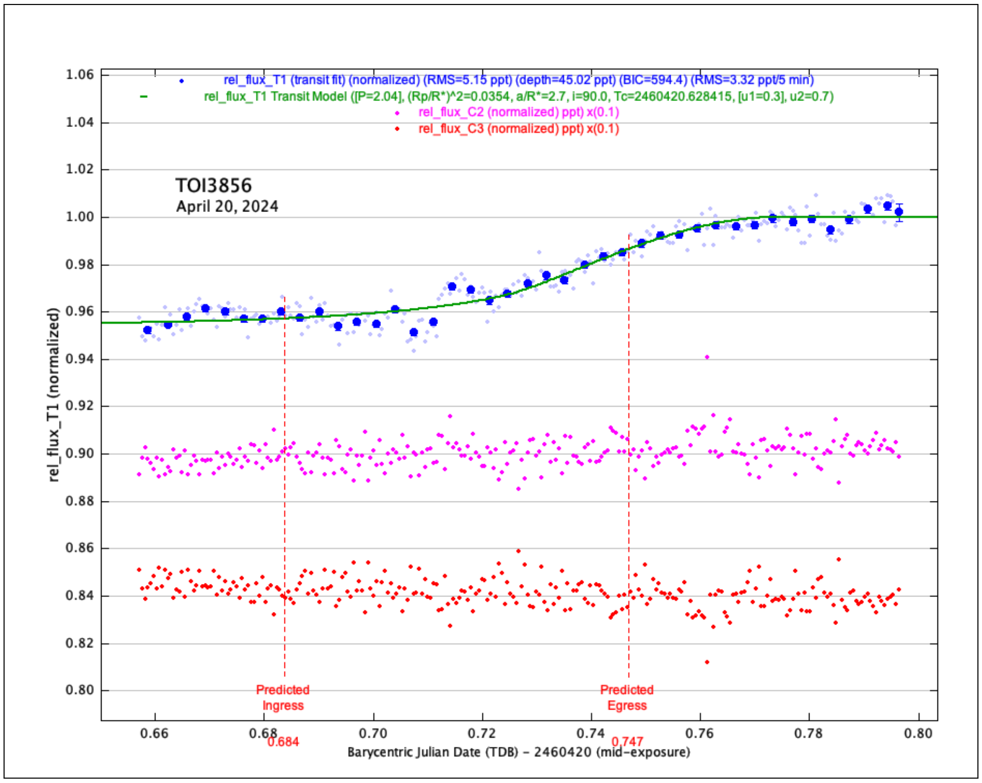

Figure 5. Light curve of TOI-3856 from April 20, 2024 where the curve shows brightness over time and is normalized to 1. Faint blue points represent each image, and the large blue points are binned points with BinSize = 5 min and error bars. The curve is plotted with a line of best fit, predicted times of ingress and egress, and arbitrarily scaled/shifted plots of the comparison stars. A 4.5% increase in brightness is shown which has a greater transit depth (or change in brightness) than the 1.3% predicted by initial TESS data[4]. Also, only the final egress in brightness is shown in the light curve, while the initial ingress is not.

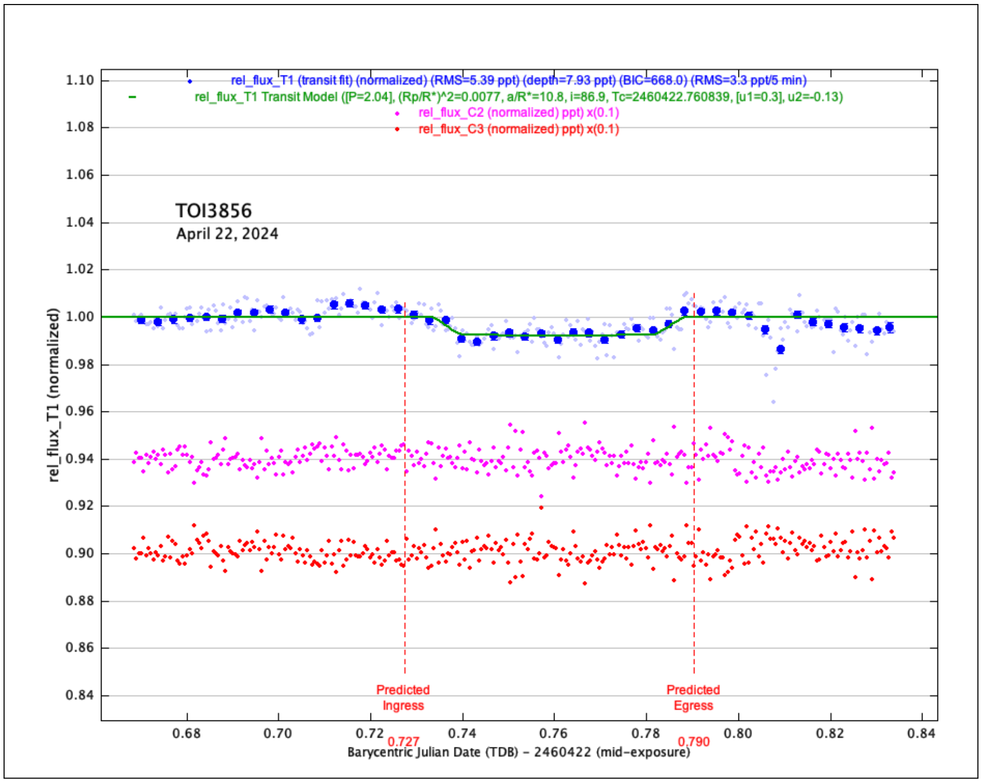

Figure 6. Light curve of TOI-3856 from April 22, 2024 where the curve shows brightness over time and is normalized to 1. Faint blue points represent each image, and the large blue points are binned points with BinSize = 5 min and error bars. The curve is plotted with a line of best fit, predicted times of ingress and egress, and arbitrarily scaled/shifted plots of the comparison stars. A singular dip in brightness, or the predicted transit shape, with a transit depth of 0.8% is shown, which is much closer to the predicted transit depth of 1.3%. It should be noted that there is a fluctuation in brightness around 0.81 BJD (TDB), but this is the result of a similar fluctuation in brightness in the comparison stars at the same time rather than the exoplanet.

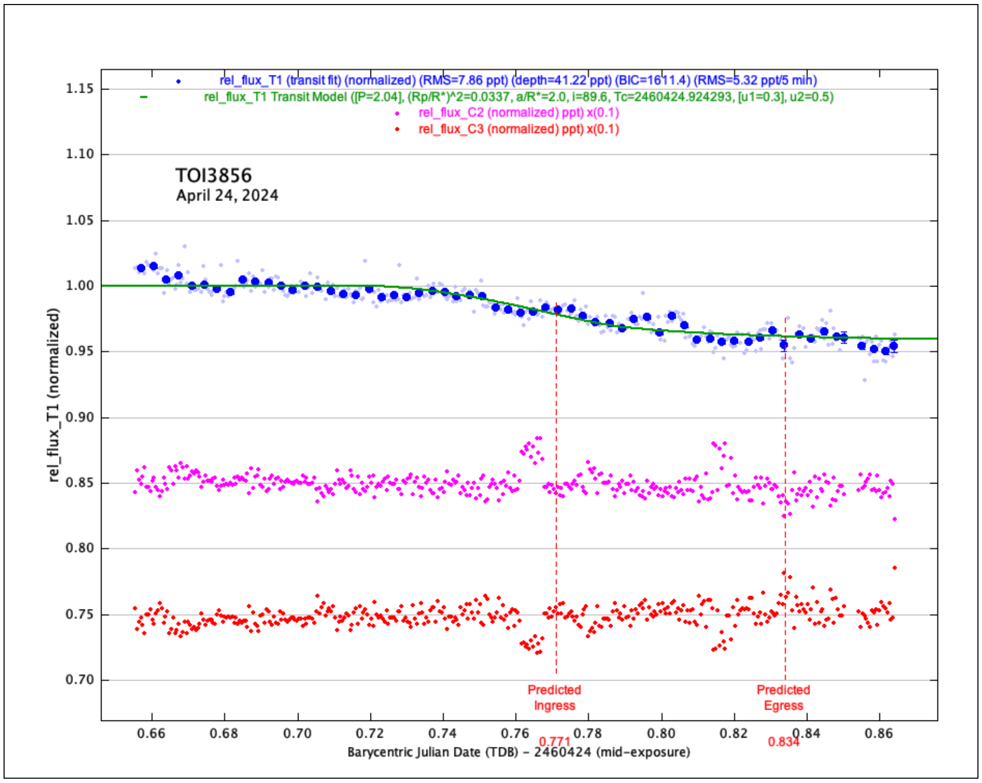

Figure 7. Light curve of TOI-3856 from April 24, 2024 where the curve shows brightness over time and is normalized to 1. Faint blue points represent each image, and the large blue points are binned points with BinSize = 5 min and error bars. The curve is plotted with a line of best fit, predicted times of ingress and egress, and arbitrarily scaled/shifted plots of the comparison stars. A 4.1% decrease in brightness is shown, which has a greater transit depth (or change in brightness) than the 1.3% predicted by initial TESS data[4], but similar to the depth in Fig. 5. It should be noted that there are small fluctuations in brightness at 0.76 and 0.82 BJD (TDB), but this is again the result of similar fluctuations in brightness of the selected comparison stars at the same time. Also, only the initial ingress in brightness is shown in the light curve, while the final egress is not.

3.2 The Impact of Comparison Star Selection on TOI-3856

When different comparison stars from the ones used in the creation of Fig. 5-7 for TOI-3856 were used, vastly different results were obtained with higher levels of noise. Two overall trends were detected in the selection of comparison stars: (1) stars that are saturated and (2) stars that are over 500 arcsec away from the target star do not serve as optimal comparison stars for reducing noise in light curves. Fig. 5 was created using comparison stars C2 and C3 (Fig. 8) where both comparison stars were not saturated (Fig. 9) and were less than 500 arcsec from the target star (Table 1). Therefore, a minimal amount of noise was found in Fig. 5, and it was used as a reference to compare the light curves in this section with. Comparison star C2 was used as a constant in the creation of the light curves in Fig. 5 and Fig. 11-13, as C2 was only 25.5 arcsec from the target star (closest star) and was not saturated (Table 1). The second comparison star used in creating those light curves was changed with each light curve; however, in Fig. 5 the second comparison star, C3, was also not saturated and less than 500 arcsec from the target star making Fig. 5 optimal for comparison.

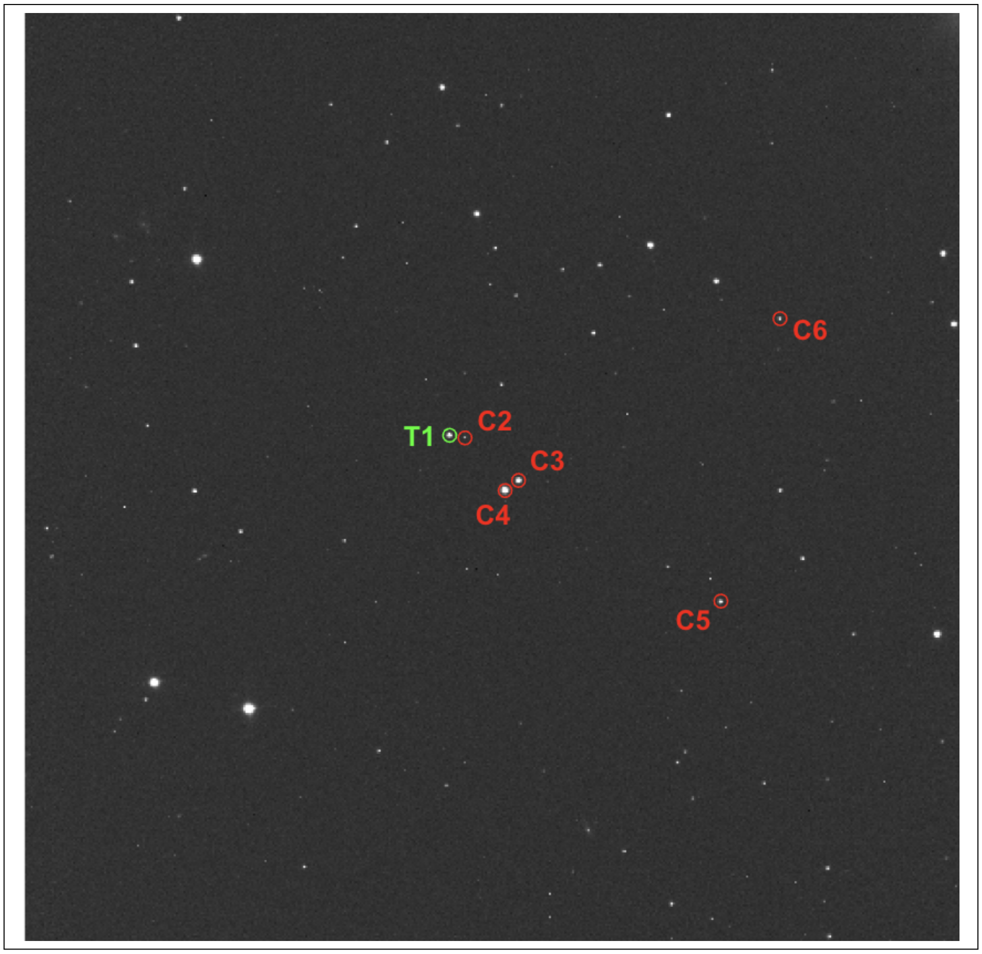

Figure 8. Sample image from the TOI-3856 data taken on April 20, 2024. Image shows target star TOI-3856 (T1) and all the comparison stars (C2-C6) used in the creation of Fig. 5, 11, 12, and 13. Each of those light curves uses comparison star C2 and comparison star C3, C4, C5, or C6, respectively. Image is 1365 pixels-by-1365 pixels (where 1 pixel = 1.15 arcsec) and is oriented with north downward and east to the right.

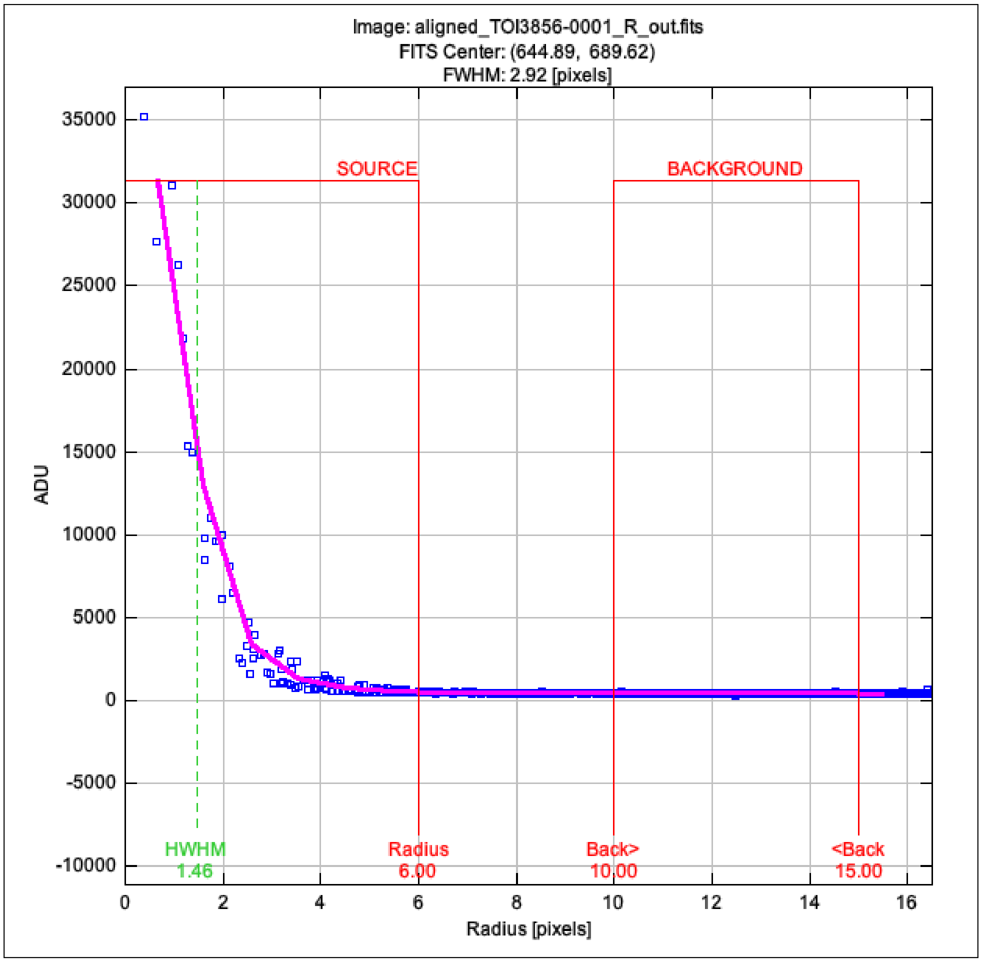

Figure 9. "Seeing profile" generated with AstroImageJ[8] for comparison star C3 (Fig. 8) used to create the light curve in Fig. 5. A "seeing profile" shows brightness in Analog to Digital Units (ADU) over distance from the center of the star. Brightness decreases from the center to edge of a star and into the background. The points near the center of the star are not plateaued, and below 45,000 ADU, indicating that the star is not saturated. All comparison stars in Fig. 8 except for C4 have similar "seeing profiles."

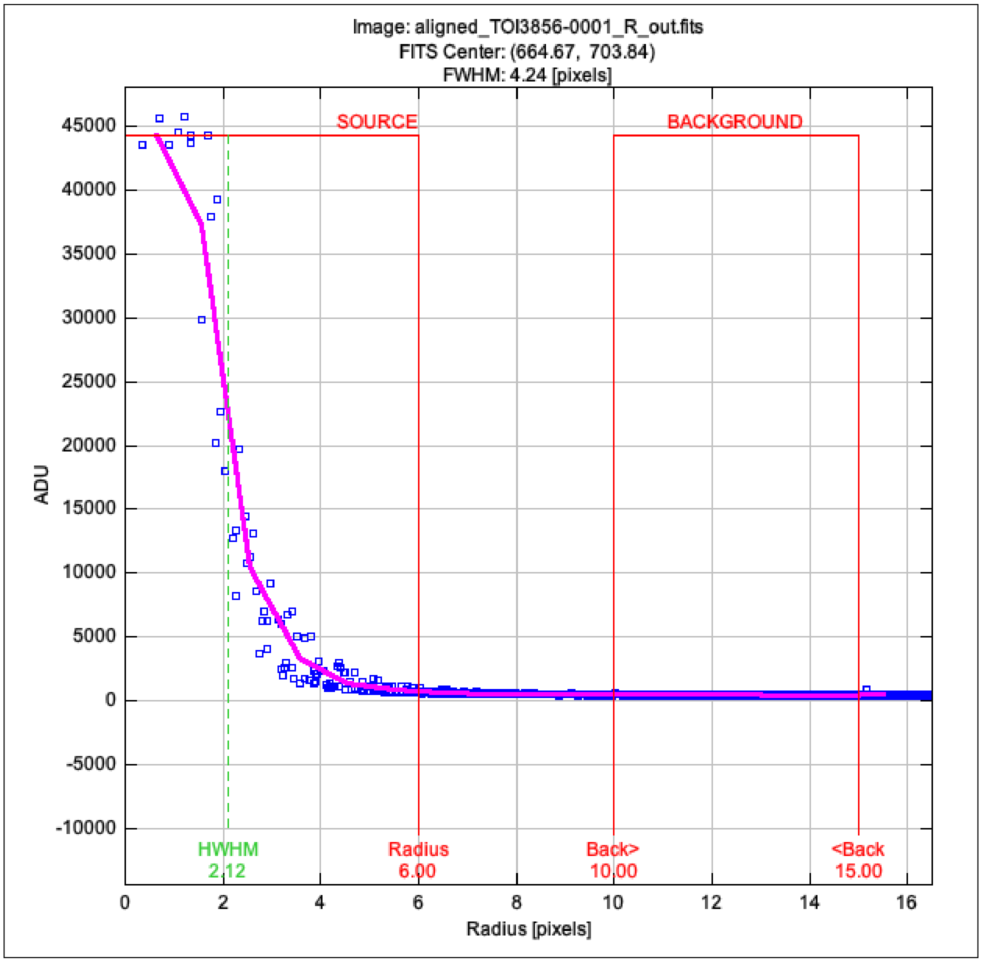

Figure 10. "Seeing profile" generated with AstroImageJ[8] for comparison star C4 (Fig. 8) used to create the light curve in Fig. 9. The points are plateaued at 45,000 ADU near the center of the star, which means the star is saturated because the pixels on the camera can only hold a maximum capacity of 45,000 ADU of light.

Light Curve	Saturated?	Distance to Target Star (arcsec)	RMS (ppt)
Fig. 5	No	135.0	5.15
Fig. 11	Yes	130.7	64.75
Fig. 12	No	531.3	13.90
Fig. 13	No	585.0	26.14

Table 1. Table provides the distance between the target star (T1) and the second comparison star (C3-C6 in order), as well as whether or not the comparison star is saturated for the light curves of TOI-3856 in Fig. 6 and Fig. 11-13. The table also provides the RMS value for each light curve.

Comparison star C4 (Fig. 8) used to create Fig. 11 is saturated because its "seeing profile" (Fig. 10) shows the star to have more than 45,000 ADU (analog to digital units) of light, which is the maximum amount of light a pixel on the telescope's camera can hold. When a pixel is saturated, the amount of light cannot be accurately measured. Therefore, this saturation of the comparison star results in a light curve (Fig. 11) with a significantly higher RMS value of 64.75 ppt than the reference light curve's (Fig. 5) RMS value of 5.15 ppt (Table 1). This comparison star is only 130.7 arcsec away from TOI-3856, so the reason for the high amount of noise in Fig. 11 is the saturation of comparison star C4.

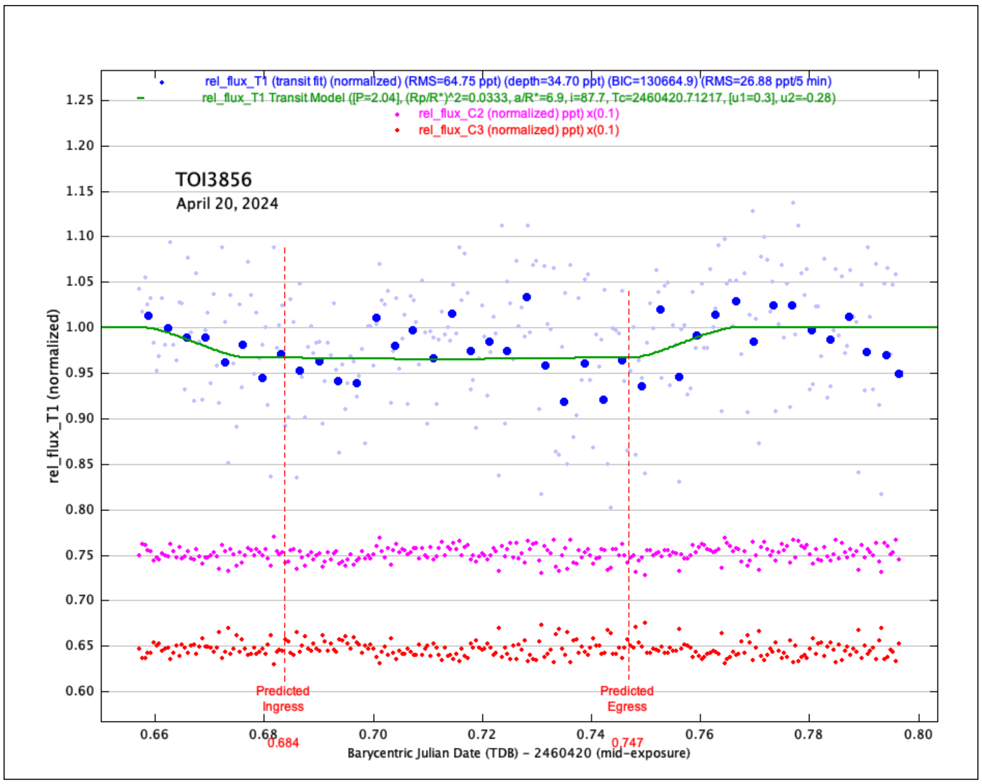

Figure 11. Light curve of TOI-3856 from observations on April 20, 2024 created with comparison stars C2 and C4 (Fig. 8) where C4 is saturated (Fig. 10). The curve shows brightness over time and is normalized to 1. Faint blue points represent each image, and the large blue points are binned with BinSize = 5 min and error bars. The curve is plotted with a line of best fit, predicted times of ingress and egress, and arbitrarily scaled/shifted plots of the comparison stars. The light curve contains high levels of noise compared to Fig. 5 with a Root Mean Square (RMS) value of 64.75 ppt and a lot of scatter in the data points.

Two other selected comparison stars for TOI-3856, C5 and C6 (Fig. 8), were not saturated, but both were greater than 500 arcsec from TOI-3856 (Table 1). As a result, the light curves of TOI-3856 made with C2 and C5/C6 (Fig. 12; Fig. 13) have larger RMS values of 13.90 ppt and 26.14 ppt (Table 1), respectively, than Fig. 5. They also both contain very brief large decreases in brightness indicating that comparison stars closer to the periphery of the images and further from target star T1–as with C5 and C6–are more likely to cause brief random fluctuations in brightness; despite the overall flux in brightness being relatively nonexistent.

These random fluctuations can also be seen in the comparison stars, which have their own changes in brightness at the same time the target star does. Note: since the first comparison star C2 (Fig. 9), which is not saturated and very close to the target star, was held constant in each light curve (Fig. 4 and Fig. 10-12), it can be assumed that the second comparison star is influencing the change in light curve shape and noise.

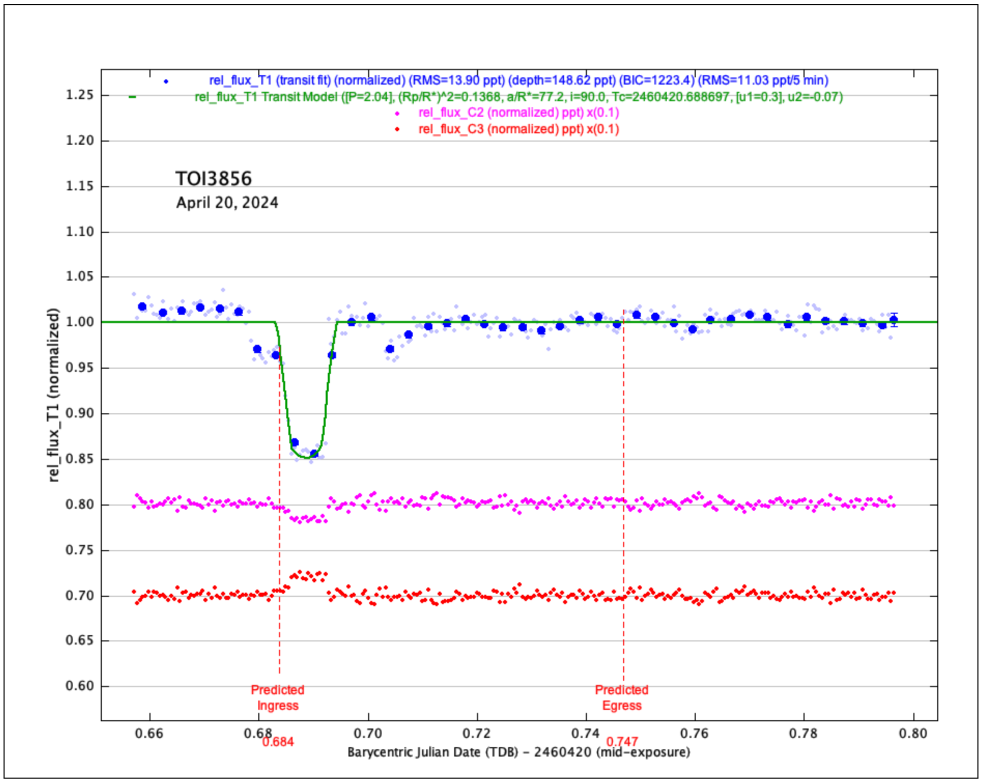

Figure 12. Light curve of TOI-3856 from observations on April 20, 2024 created with comparison stars C2 and C5 (Fig. 8) where C5 is not saturated but is at a distance of 531.3 arcsec from the target star (Table 1). The light curve has higher noise levels than Fig. 5 and an RMS value of 13.90 ppt, which is the result of a brief large decrease in brightness. At the same moment, there are brief fluctuations in brightness of the comparison stars. Note that the curve shows brightness over time and is normalized to 1. Faint blue points represent each image, and the large blue points are binned with BinSize = 5 min and error bars. The curve is plotted with a line of best fit, predicted times of ingress and egress, and arbitrarily scaled/shifted plots of the comparison stars.

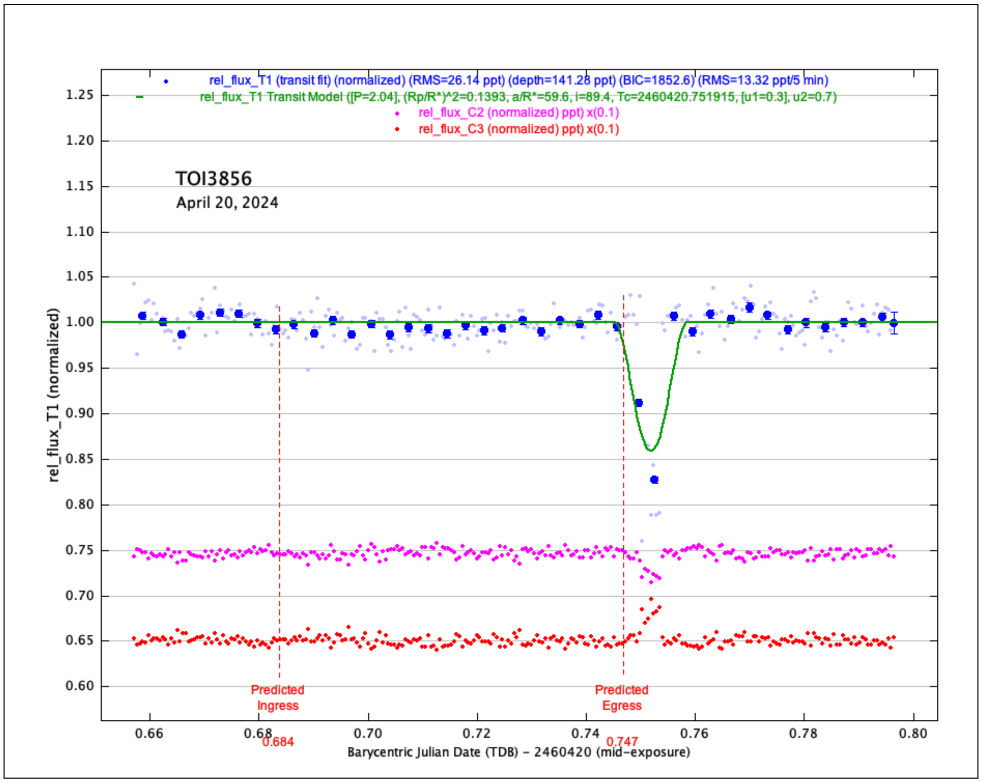

Figure 13. Light curve of TOI-3856 from observations on April 20, 2024 created using comparison stars C2 and C6 (Fig. 8) where C6 is not saturated but is at a distance of 585.0 arcsec from the target star (Table 1). The light curve has higher noise levels than Fig. 5 and an RMS value of 26.14 ppt, which is the result of a brief large decrease in brightness. Again there are fluctuations in brightness of the comparison stars at the same moment. Note that the curve shows brightness over time and is normalized to 1. Faint blue points represent each image, and the large blue points are binned with BinSize = 5 min and error bars. The curve is plotted with a line of best fit and predicted times of ingress and egress.

3.3 Planetary Radius Calculations

The portion of light blocked by the transiting planet is equal to the ratio of planet-to-star areas. Therefore, to calculate the radius of each candidate the following equation was derived for transit depth δ, or the change in brightness:

$$\begin{aligned}\delta &= \frac{A_p}{A_s} \\ &= \frac{\pi R_p^2}{\pi R_s^2} \\ \delta &= \left(\frac{R_p}{R_s}\right)^2 \qquad (1)\end{aligned}$$

δ is the transit depth which AstroImageJ calculated for each light curve in parts per thousand (ppt). R_p is the planetary radius that was solved for and R_s is the stellar radius, which was given from initial TESS data[4]. Equation 1 was rearranged to solve for planetary radius:

$$R_p = R_s\sqrt{\delta} \tag{2}$$

However, there are errors on both the transit depth, as shown by the RMS value, and the stellar radius, as given by error values from TESS data[4]. Therefore, those error values impacted the uncertainty of the calculated planet radius so error propagation had to be accounted for. To do so, the planet radius error was estimated using the partial derivative of the planetary radius with respect to each of the uncertainties. The following formula for error propagation was used where σ is the error value, x is the calculated variable, and u and v are the variables with uncertainties[9]:

$$\sigma_x^2 = \sigma_u^2\left(\frac{\partial x}{\partial u}\right)^2 + \sigma_v^2\left(\frac{\partial x}{\partial v}\right)^2 + \ldots \tag{3}$$

Using Equation 3, the equation for planet radius error σ_{R_p} was derived with transit depth error σ_δ, or RMS value, and stellar radius error σ_{R_s}, or the plus or minus value from TESS data. The partial derivative with respect to δ and R_s of Equation 2 was taken.

$$\begin{aligned}
\sigma_{R_p}^2 &= \sigma_\delta^2\left(\frac{\partial R_p}{\partial \delta}\right)^2 + \sigma_{R_s}^2\left(\frac{\partial R_p}{\partial R_s}\right)^2 \\
\sigma_{R_p}^2 &= \sigma_\delta^2\left(\frac{R_s}{2\sqrt{\delta}}\right)^2 + \sigma_{R_s}^2\left(\sqrt{\delta}\right)^2 \\
\sigma_{R_p} &= \sqrt{\sigma_\delta^2\left(\frac{R_s^2}{4\delta}\right) + \sigma_{R_s}^2\delta}
\end{aligned} \tag{4}$$

Next, Equation 2 and Equation 4 were used to calculate the planet radius and error on planet radius, respectively, for each exoplanet. Given values for stellar radius and error[4] and values from the light curves (Fig. 3; Fig. 4; Fig. 6) were used (Table 2). Therefore, the following planetary radii (in Jupiter radius) were determined:

$$\begin{aligned}
R_{\text{TOI-1858}} &= 1.00 \pm 0.19\ \text{R}_\text{J} \\
R_{\text{TOI-1832}} &= 0.82 \pm 0.32\ \text{R}_\text{J} \\
R_{\text{TOI-3856}} &= 1.00 \pm 0.34\ \text{R}_\text{J}
\end{aligned}$$

Object	δ (ppt)	σ_δ (ppt)	R_s (R_J)	σ_{R_s} (R_J)
TOI-1858	16.89	5.85	7.66	0.7
TOI-1832	11.15	8.42	7.76	0.6
TOI-3856	7.93	5.39	11.24	0.6

Table 2. Table provides values for transit depth (δ) and error on transit depth (σ_δ) from the light curves of all three targets (Fig. 3; Fig. 4; Fig. 6) to be used in planetary radius calculations. Table also provides the given values for stellar radius (R_s) and error on stellar radius (σ_{R_s}) from literature[4] to be used in planetary radius calculations.

4 Discussion

It can be concluded that TOI-1858, TOI-1832, and TOI-3856 all contain exoplanet candidates that are now confirmed to exist due to the singular dip in brightness from transit photometry (Fig. 3; Fig. 4; Fig. 6). These three confirmed planets have planetary radii of 1.00 ± 0.19 R_J, 0.82 ± 0.32 R_J, and 1.00 ± 0.34 R_J, respectively, where R_J stands for Jupiter radius. From transit photometry it can also be concluded that TOI-1832 potentially contains an additional exoplanet in the star system due to possible transit timing variations, but further transit observations are needed to confirm the timing variations. And it can be concluded that TOI-3856 contains some larger unknown object as a result of the larger than predicted transit depth (Fig. 5 and Fig. 7), which could be a transiting exoplanet in a multi-planetary system. Finally, it can be concluded that when choosing comparison stars to produce light curves of exoplanet transit observations, stars that are not saturated and less than 500 arcsec away from the target star should be used.

The results of this study could have been limited by noise in the light curve. In transit photometry with ground-based telescopes, noise can come as a result of atmospheric interference and noise in the detector. Calibration frames were used to reduce systematic noise, but they are not perfect and could not eliminate all noise as evident by the RMS values. Therefore, the precision of the model fits could have been negatively impacted. However, the RMS values in the light curves used (excluding the poor comparison star examples) are fairly low so the conclusions drawn are still relatively accurate. Also, an error was calculated for each planetary radius using the RMS value to take into account any noise in the light curve.

Confirming exoplanet candidates, and finding additional planets through transit timing variations, is how astronomers create a list of confirmed exoplanets. With new confirmed exoplanets, like the three in this study, astronomers can look at their atmospheres and compositions using using telescopes like JWST to search for potentially habitable planets. Astronomers can also study the orbital architectures of multi-planetary systems found through transit timing variations, or the method used for TOI-3856, to better understand how Earth's Solar System is unique from or similar to other multi-planetary systems. Additionally, a set of guidelines for choosing comparison stars is necessary for any future transit observations.

Further research is necessary to perform radial velocity measurements of TOI-1858, TOI-1832, and TOI-3856 in order to determine the mass of the confirmed exoplanets, which can also give insight into the density of the planets when combined with the radii calculations. Additional research is also needed to perform spectroscopic observations with telescopes, such as JWST, to examine the atmospheres and compositions of these planets. Radial velocity measurements and spectroscopic observations are beyond the scope of the resources available to the competition entrant because of the need for a high quality spectrometer. Finally, future research, in the form of follow-up transit observations and radial velocity measurements, is necessary to confirm the additional planet found from potential transit timing variations in the TOI-1832 system and to investigate the unknown object in the TOI-3856 system.

5 Acknowledgments

Dr. Don McCarthy, Christine Leventhal, and David Lewis.

References

1. G. R. Ricker, J. N. Winn, R. Vanderspek, et al. Transiting exoplanet survey satellite. *JATIS*. **1**, 014003 (2015).

2. R. Hounsell. How to find an exoplanet-user version. https://heasarc.gsfc.nasa.gov/docs/tess/HowToFindAnExoplanet-UserVersion.html (2018).

3. K. A. Collins, K. I. Collins, J. Pepper, et al. The KELT follow-up network and transit false-positive catalog: Pre-vetted False Positives for TESS *AJ*. **156**, 234 (2018).

4. K. G. Stassun, R. J. Oelkers, M. Paegert, et al. The revised TESS input catalog and candidate target list. *AJ*. **158**, 138 (2019).

5. J. P. Gardner, J. C. Mather, R. Abbott, et al. The james webb space telescope mission. *Publications of the Astronomical Society of the Pacific*. **135** 068001 (2023).

6. N. M. Guerrero, S. Seager, C. X. Huang, et al. The TESS object of interest catalog from the TESS prime mission. *ApJS*. **254**, 39 (2021).

7. M. Kunimoto, T. Daylan, N. Guerrero, et al. The TESS faint-star search: 1617 TOIs from the TESS primary mission. *ApJS*. **269**, 33 (2022).

8. K. A. Collins, J. F. Kielkopf, K. G. Stassun, F. V. Hessman. AstroImageJ: Image processing and photometric extraction for ultra-precise astronomical light curves. *AJ*. **153**, 77 (2017).

9. H. Ku. Notes on the use of propagation of error formulas. *JRNBS*. **70C**, 263 (1966).

10. E. Jensen. Tapir: A web interface for transit/eclipse observability. *Astrophysics Source Code Library, record ascl:1306.007* (2013).

11. D. Lang, D. W. Hogg, K. Mierle, M. Blanton, S. Roweis. Astrometry.net: Blind astrometric calibration of arbitrary astronomical images. *AJ*. **139**, 1782 (2010).

12. N. Akhand, S. Atwa, J. Boehm, M. Eaton, C. Ho, V. Markovich, K. Raharjo, A. Rahbar, A. Shellhammer, A. Xu. Ground-based photometry followup for transiting exoplanet candidate TOI-1516b. *JRASC*. **117**, 141 (2023).